



Field of studies: Geoinformation

Album ID: 455828

Tomasz Matuszek

**Measuring an impact of the Landsat 8 thermal
band on the supervised land cover classification
results**

*Ocena wpływu zastosowania kanału termalnego
Landsat na wyniki nadzorowanej klasyfikacji pokrycia
terenu*

Engineer's thesis written
in the Institute of Geoecology and Geoinformation
under the supervision of
dr hab. Jakub Nowosad

Poznań, 2023

Abstract

Abstract

Accurate land cover maps are crucial in many fields of geography, urban planning and environmental studies. Currently, the most popular method to create such maps is the usage of machine learning techniques and satellite imagery. Researchers still investigate different variables and approaches in strive to achieve the highest possible accuracy of their predictions. The goal of this study was to evaluate importance of thermal band acquired from Landsat 8 programme for land cover mapping. LUCAS land cover reference dataset was used to fit the Random Forest model. Apart from training the model, several machine learning techniques such as hyperparameter tuning, nested spatial cross-validation and benchmarking were performed in order to achieve possibly high and accurate performance measures. Moreover, thermal band's importance on model results was investigated. Analysis the of variable importance showed that impact of the land surface temperature was not very high, but indeed visible. Moreover, I discovered that thermal band had significantly higher impact on the model prediction when classifying artificial land. These findings suggest that thermal information may be influential in the mapping development of urban areas. However, further studies involving spatio-temporal analysis for more study areas are needed to quantify thermal band's impact more precisely.

Keywords: machine learning, remote sensing, variable importance, land surface temperature

Abstrakt

Dokładne mapy pokrycia terenu mają kluczowe znaczenie w wielu dziedzinach geografii, urbanistyki i badań środowiskowych. W ostatnich latach najpopularniejszą metodą tworzenia takich map jest wykorzystanie zobrazowań satelitarnych oraz technik uczenia maszynowego. Naukowcy wciąż badają zastosowanie różnych zmiennych i podejście, dając do osiągnięcia jak najwyższej dokładności swoich modeli. Celem niniejszej pracy była ocena znaczenia kanału termalnego pozyskanego z satelity Landsat 8 w tworzeniu map pokrycia terenu. Do stworzenia modelu lasu losowego wykorzystano zbiór danych o pokryciu terenu pozyskany w ramach programu LUCAS. Poza treningiem modelu, w celu uzyskania możliwie wysokiej jakości modelu i dokładnej jego oceny, zastosowano techniki uczenia maszynowego, takie jak optymalizacja parametrów, kroswalidacja przestrzenna oraz benchmarking. Ponadto, zbadano znaczenie kanału termalnego na wyniki modelu. Analiza istotności zmiennych wykazała, że wpływ temperatury nie był wysoki, ale jednak widoczny. Co więcej zauważono, że kanał termalny miał znacznie większy wpływ na wyniki modelu dla klasyfikacji obszarów zabudowanych. Wyniki te sugerują, że informacja termiczna może mieć wpływ na lepsze mapowanie rozwoju obszarów miejskich. Jednakże aby dokładniej określić wpływ kanału termalnego, potrzebne są dalsze badania obejmujące analizę przestrzenno-czasową dla większej liczby obszarów badawczych.

Słowa kluczowe: uczenie maszynowe, teledetekcja, istotność zmiennych, temperatura powierzchni

Contents

| | |
|---|-----------|
| Abstract | 3 |
| 1 Introduction | 7 |
| 2 Materials and methods | 9 |
| 2.1 Satellite imagery | 11 |
| 2.2 Land cover data | 12 |
| 2.3 Machine learning | 15 |
| 2.4 Variable importance and its spatial distribution | 20 |
| 2.5 R language environment | 24 |
| 3 Land cover map | 25 |
| 4 Assessing model quality | 29 |
| 5 Evaluating thermal band's impact | 31 |
| 5.1 Measuring importance of thermal band | 32 |
| 5.2 Spatial distribution of thermal band's importance | 37 |
| 6 Conclusions | 41 |

Chapter 1

Introduction

Land cover is a physical characteristic of Earth's surface describing distribution of vegetation, water, soil and other features on the ground (Rawat et al., 2015). The production of accurate land cover maps is crucial for conducting spatial analyses, studying environmental changes (Reis, 2008) and evaluating urban development (Hashem et al., 2015). Land cover information is also useful for the general circulation models (GCM) development (Running, 2008) and has been selected as one of the most essential variables that contribute to describing Earth's environment and climate (Bojinski et al., 2014).

The main method of creating land cover maps is based on multispectral satellite data and remote-sensing methods. The two most popular, free-of-charge sources of satellite imagery are Landsat programme (run by NASA and USGS) and Sentinel programme (conducted by ESA). These datasets are usually utilized to create classification models based on machine learning techniques, which gained popularity in the recent years (Maxwell et al., 2018). A supervised machine learning model, including the one used in this study, analyzes training set containing labels of land cover classes and tries to learn how to recognize them.

Over the past few years, there were several attempts to automate creation of land cover maps (Malinowski et al., 2020; Witjes et al., 2021). An automated workflow, however, requires high understanding of every step of machine learning process and appropriate choice of explanatory variables. Spectral bands and spectral indices are

the most commonly used variables. However, some satellites like Landsat 8, have a thermal sensor as well, which measures land surface temperature (LST) of the Earth. There is a significant interaction between LST and extent of urban and impervious areas (Dutta et al., 2019), thus we can assume that this variable might be influential on the classification model results. Thermal band's impact on the model results is described in several studies, for example, Rodríguez-Galiano et al. (2012), Zhao et al. (2019), Sun et al. (2015). However, despite adding completely new information compared to spectral bands, the thermal band is noticeably more often omitted in classification models, probably due to its coarser resolution (Rodríguez-Galiano et al., 2012). Because of this, its impact on model predictions is not clear enough and needs further research.

The main goal of this study is to evaluate thermal band's impact on a classification model, study its spatial distribution and try to give broader knowledge of how it should be used. Random Forest model will be trained on a dataset for Poland and a land cover map of Poznań metropolitan area will be created. Then, both the machine learning model and the result map will be used to measure thermal band's impact on the classification results.

Chapter 2

Materials and methods

Workflow of the study consisted of several stages: preprocessing of source data (described in Sections 2.1 and 2.2), creating a training dataset, model parameters tuning and model quality assessment (Section 2.3.2), land cover map prediction and evaluating the impact of the thermal band on the model results (Section 2.4). Visual representation of the workflow is shown in Figure 2.1.

Each of these steps was performed using R programming language (R Core Team, 2021) and final visualizations were created in QGIS software (QGIS Development Team, 2009). Both programming environment and GIS software used in this process are open-source.

Landsat ARD dataset, provided by GLAD laboratory at the University of Maryland, was used as a source of multi-spectral satellite imagery (Potapov et al., 2020). Training points were obtained from LUCAS dataset created by Eurostat (d'Andrimont et al., 2020). Both datasets were downloaded for central-western part of Poland which was chosen as the training area (Figure 2.2). This data was preprocessed and then used to train the model and validate its performance.

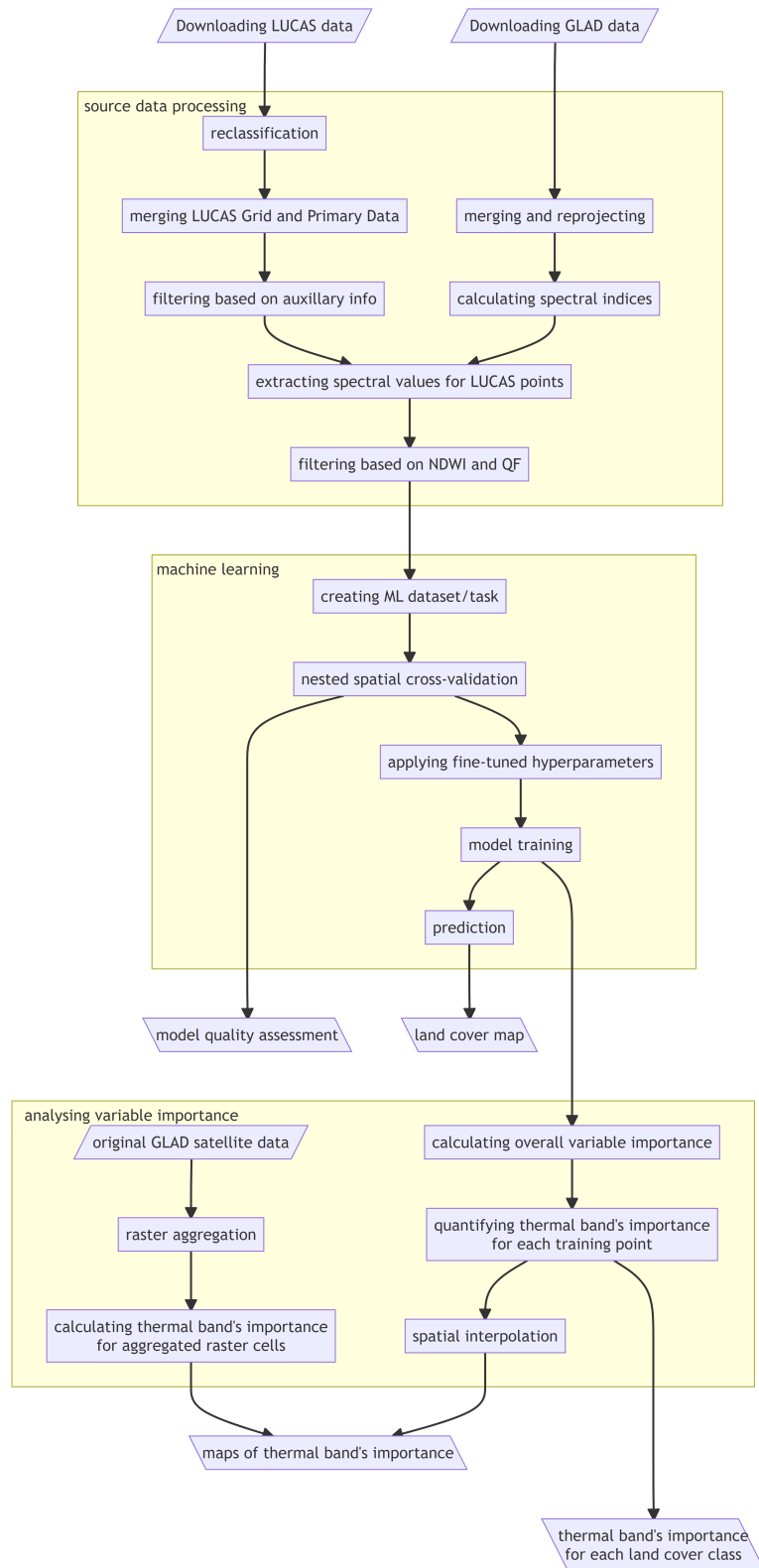


Figure 2.1: General workflow of the study

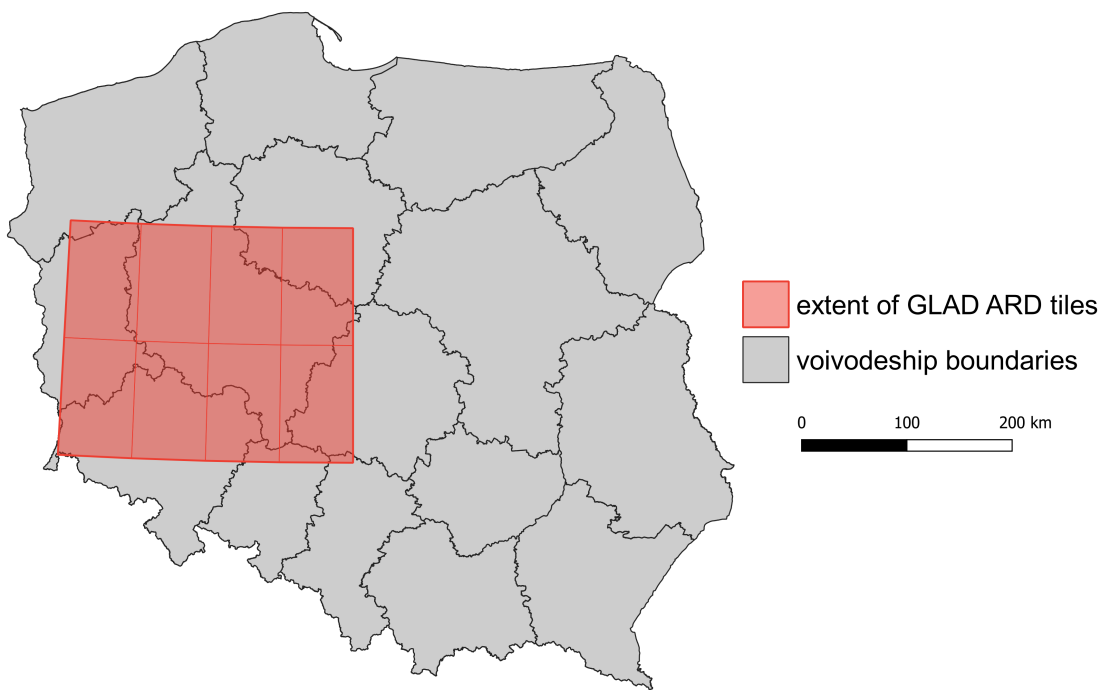


Figure 2.2: Area covered by the downloaded satellite imagery

2.1 Satellite imagery

Satellite imagery from GLAD Landsat ARD product is available in 16-day interval composites and is divided into $1^\circ \times 1^\circ$ tiles. Processing of original Landsat images performed by the GLAD team included converting spectral bands' information to top-of-atmosphere (TOA) reflectance, converting thermal band values to brightness temperature (BT) in Kelvins, scaling the values of all bands, as well as, adding quality flag (QF) for every pixel (Potapov et al., 2020).

Satellite images for eight $1^\circ \times 1^\circ$ tiles, covering the study area, were downloaded using GLAD Tools v1.1 and PERL programming language (Figure 2.1). These images are from 10th interval of the year 2018, so downloaded mosaics consist of images acquired between 24.05.2018 and 8.06.2018. All downloaded images were merged and reprojected from the WGS 84 coordinate reference system (EPSG:4326) to UTM zone 33N (EPSG:32633). Every band was also resampled from its original 0.00025° resolution (corresponding to 27.83 m on the equator) to 30 meters.

Table 2.1: Formulas of spectral indices derived from Landsat data

| band/index | abbreviation | formula |
|--|--------------|---------------------------------------|
| Blue | B2 | - |
| Green | B3 | - |
| Red | B4 | - |
| Near Infrared | B5 (NIR) | - |
| Short-wave Infrared 1 | B6 (SWIR1) | - |
| Short-wave Infrared 2 | B7 (SWIR2) | - |
| Thermal | B10 (TIRS1) | - |
| Normalized Difference Vegetation Index | NDVI | (B5 - B4) / (B4 + B5) |
| Modified Normalized Difference Water Index | MNDWI | (B3 - B6) / (B3 + B6) |
| Normalized Difference Moisture Index | NDMI | (B5 - B6) / (B5 + B6) |
| Modified Bare Soil Index | MBI | (B6 - B7 - B5) / (B6 + B7 + B5) + 0.5 |

In addition, four spectral indices were derived: Normalized Difference Vegetation Index (NDVI: Tucker, 1979), Modified Normalized Difference Water Index (MNDWI: Xu, 2006), Normalized Difference Moisture Index (NDMI: Jin et al., 2005) and Modified Bare soil Index (MBI: Nguyen et al., 2021). Formulas used to calculate these indices can be found in Table 2.1.

2.2 Land cover data

Data collected during the LUCAS field survey performed by Eurostat was chosen as a land cover training set. At the moment of writing, it is the most accurate and comprehensive dataset containing information about land use and land cover (Pflugmacher et al., 2019) due to the fact that every point was either manually photo-interpreted or assessed during an *in-situ* visit.

LUCAS field survey consists of two phases. The first phase is based on a grid of points with 2 km spacing covering whole territory of the European Union (which equals to more than 1 million points). Each point of the grid is visually interpreted using ortho-photos or satellite images, and classified into one of seven major land-cover classes. These classes are: arable land, permanent crops, grassland, wooded areas/shrub land, bare

land, artificial land and water (Buck et al., 2015). In the second phase, a subsample of grid points is selected and then visited by Eurostat surveyors. They classify each point according to full LUCAS land cover and land use classification. The survey takes place in the spring and summer in order to observe chosen places in their high vegetation season (d'Andrimont et al., 2020).

Surveyors not only assign land cover and land use classes to points, but they also add auxillary information such as plant species present at the site, percentage of land coverage of a chosen class, height of the trees and their maturity, as well as information about local water management and irrigation. If there are more than one land cover/land use types at the point, observer can also assign a secondary class for every LUCAS point (Buck et al., 2015).

The majority of the training points used in the classification model were from the second phase of LUCAS survey, also called LUCAS Primary Data. I downloaded a total of 4,153 points for the study area. The pre-processing step included omitting records with missing data, excluding artificial linear land cover classes (e.g. roads or railways) and excluding points that were surveyed more than 500 meters from their theoretical location. In the next step, detailed land cover classes were aggregated into eight main groups of land cover types. Two of them - grassland and shrubland were additionally aggregated into one land cover class due to their spectral and descriptive similarity. Then, I filtered some of the points according to the percentage of land cover class coverage or percentage of impervious surface coverage (Table 2.2). This step reduced number of unreliable training points with mixed land cover, e.g. points with assigned class covering less than 50% of surface around it.

For the least frequent classes in the LUCAS Primary Data dataset - bare land, artificial land and water bodies - I also added points classified during the first phase of LUCAS survey (Figure 2.3). This step was necessary to ensure that every land cover class is represented by enough points. It was not possible only for the wetlands class, because of the lack of such category in the first phase classification. At the end of the pre-processing, dataset had 3,778 training points.

Table 2.2: Filters applied to reclassified land cover groups. IMP - impervious surface, HRB - herbaceous plants cover, TC - tree cover

| ID | LC class | LUCAS Grid | LUCAS Primary Data | Filters |
|----|-----------------|----------------------|----------------------------------|-----------------------|
| 1 | arable land | - | B00 (Cropland) | <30% IMP |
| 2 | grassland | - | E00 (Grassland), D00 (Shrubland) | >50% HRB; <30% IMP |
| 3 | forests | - | C00 (Woodland) | >50% TC; <20% IMP |
| 4 | bare land | 6 (Bare surface) | F00 (Bare land) | - |
| 5 | artificial land | 7 (Artificial areas) | A00 (Artificial land) | >70% IMP |
| 6 | water bodies | 8 (Inland water) | G00 (Water areas) | - |
| 7 | wetlands | - | H00 (Wetlands) | - |

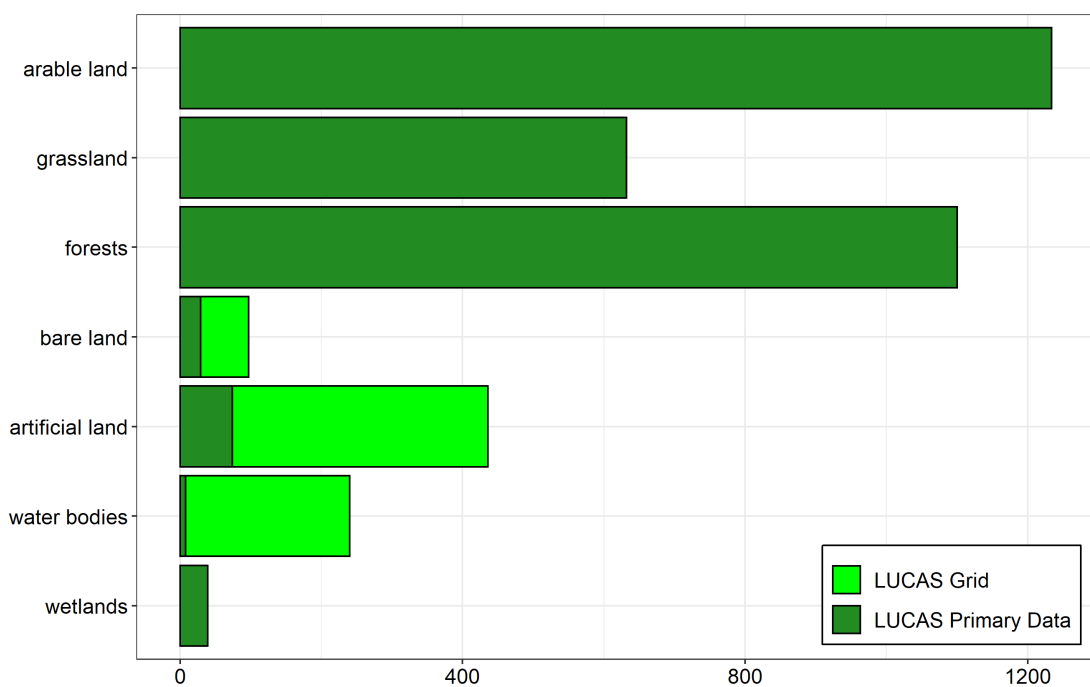


Figure 2.3: Distribution of points by land cover class after pre-processing

After extracting values from Landsat ARD raster, LUCAS points were also filtered using the quality flag provided. Only points with the clear-sky quality flag were taken into account during the model training. Moreover, water bodies points in which NDWI was lower than 0 were also excluded. These two conditions eliminated 404 points in total.

The training set obtained after pre-processing can be seen in Figure 2.4. Spatial distribution of data points was fairly even and due to the structure of LUCAS data set, every point was located 2 kilometers or further from the next one.

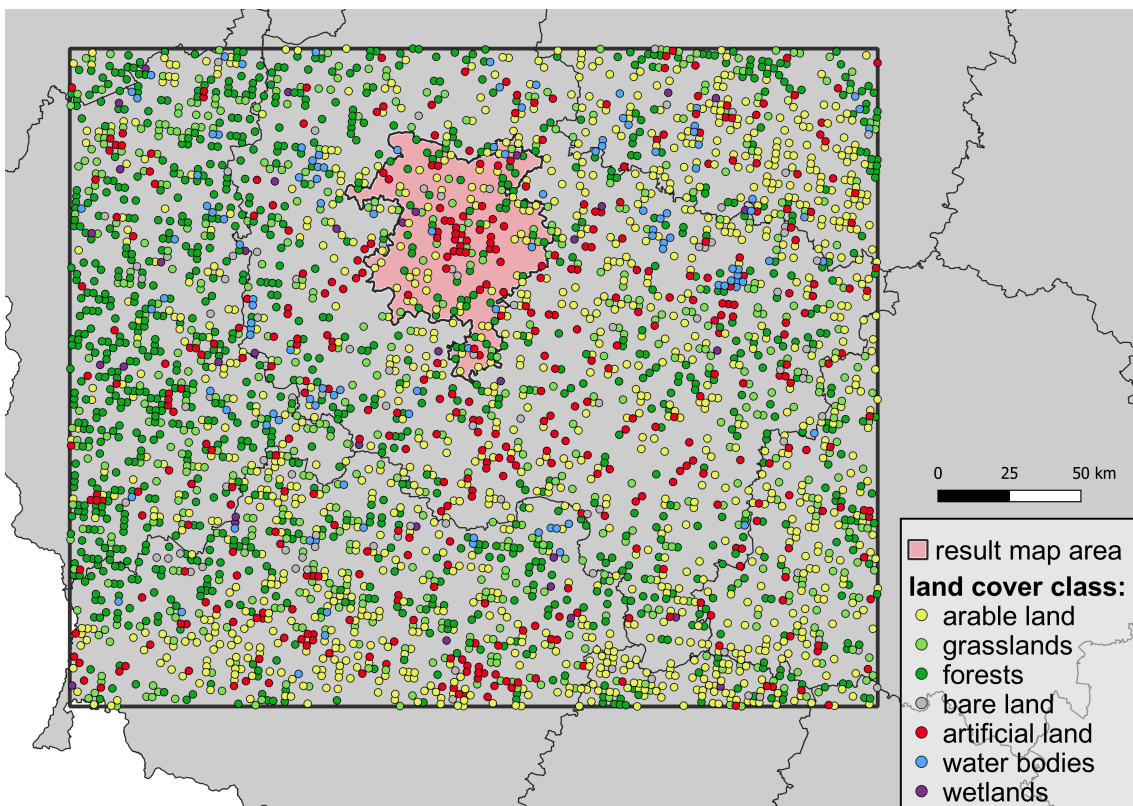


Figure 2.4: Spatial distribution of LUCAS training points after pre-processing

2.3 Machine learning

Machine learning is a computation method used to teach machines from datasets automatically, without being specifically programmed (Mahesh, 2018; Sarker, 2021). We can divide machine learning methods into two main groups: supervised and unsupervised.

Unsupervised learning analyzes unlabeled datasets without the need for human intervention. This is widely used for extracting generative features, identifying meaningful trends and structures, grouping results and exploratory purposes (Sarker, 2021). This type of machine learning discovers hidden patterns or data groupings (clusters) which is used in exploration analysis or objects segmentation.

Supervised learning uses labeled training data and a collection of training examples, which are used by an algorithm to find relationships between different variables. It is carried out when certain goals are identified to be accomplished from a certain set of

inputs. There are two main types of supervised learning tasks: classification (separating data) and regression (fitting data) (Sarker, 2021).

In this study, supervised classification algorithm called Random Forest (RF) was used (Breiman, 2001).

2.3.1 Random forest algorithm

I chose Random Forest as an algorithm used in this study, since it is considered to be the best classification algorithm for land cover mapping (Talukdar et al., 2020). It is a very popular machine learning tool thanks to its high interpretability and relatively high accuracy (Qi, 2012). Other advantages of this algorithm is its ability to handle missing values, wide spectrum of accepted variable types (continuous, binary, categorical) and ease of modelling high-dimensional data (Qi, 2012). Random Forest consists of a specified number of decision trees, which are based on series of splitting rules.

A decision tree aims to partition the dataset into smaller, more homogeneous groups (Kuhn et al., 2013). This process creates a set of rules by dividing dataset into several categories. Each rule in the decision tree is specified by a feature (variable used to split) and a threshold (value of a feature dividing dataset) (Sekulić et al., 2020). Random Forest algorithm is characterized by using many decision trees at the same time and receiving results by applying majority voting system based on outputs of all decision trees (Kuhn et al., 2013). Each tree in the forest has slightly different input data - a subset of data is sampled with replacement to get different result in every tree. This process is known as bagging or bootstrap aggregating (Schonlau et al., 2020). Moreover, algorithm is allowed to use only a subset (randomly sampled) of available variables in every split which reduces correlation between trees (Sohil et al., 2022).

2.3.2 Model quality assessment and fine-tuning

Accuracy of the model was assessed using five performance measures:

- Overall accuracy: ratio of number of correct predictions to the total number of input points
- Kappa coefficient: how well the classification performed as compared to assigning values randomly
- Recall (producer's accuracy): how often are real features on the ground correctly shown on the classified map
- Precision (user's accuracy): how often the class on the map will actually be present on the ground
- F1-score: harmonic mean between precision and recall, measures if classifier both classifies data correctly and does not miss a significant number of points

Every above metric, except Kappa coefficient, takes values from 0 to 1. Value of 0 means poor model performance and value of 1 means high quality of the model. As for Kappa coefficient, its values range from -1 to 1. Values below 0 mean worse agreement between data distributions than random chance and values above 0 (up to 1) mean model performing better than random.

Values of these indices were estimated with the help of resampling technique called spatial cross-validation (CV) (Lovelace et al., [2019](#)). It is a type of cross-validation that divides dataset into folds and also considers spatial aspect of the data.

In k -fold cross-validation, every data point is used in both training and testing set. Whole dataset is randomly divided into k equal parts (*folds*). Then, machine learning model is independently trained k times and in each run, different part of the dataset is used as validation set, while remaining $k - 1$ parts are used to fit the model. This way, every data point is used in the testing set only once and is used to train the model in the remaining runs (Jiao et al., [2016](#)). Usually, whole cross-validation procedure is repeated several

times to get higher number of unique dataset splits and to receive more reliable average values of the overall accuracy (Varga et al., 2021). Such approach is a compromise which enables possibility of using a whole dataset in the training process of the final model without a need of acquiring independent testing set in order to measure model's performance.

Since this study is based on geographic data, spatial autocorrelation needs to be taken into account. As Tobler stated: "Everything is related to everything else, but near things are more related than distant things" (Tobler, 1970). In order to prevent testing points from being related to training points, I applied spatial cross-validation approach which aims to prevent the model to overfit to the training data. This method is different than regular cross-validation only in the partitioning step - instead of randomly dividing dataset into groups, location of data points is used together with k-means clustering (Brenning, 2012) in order to create spatially disjoint folds (Lovelace et al., 2019). Thanks to this partitioning method, spatial bias can be significantly reduced which leads to more reliable performance estimation. Example of such approach can be seen in Figure 2.5.



Figure 2.5: Comparison of random and spatial partitioning of dataset for cross-validation on external example data (Source: Lovelace et al., 2019)

Table 2.3: *Hyperparameters of RF model optimized during nested spatial cross-validation*

| Hyper-parameter | Search space | Optimal value |
|-----------------|--------------|---------------|
| number of trees | 50 - 400 | 186 |
| maximum depth | 10 - 40 | 99 |
| min. node size | 1 - 10 | 2 |

Random Forest algorithm takes several hyperparameters as an input in order to specify how much should it fit to training data. Optimizing these parameters is crucial for tree-based machine learning models (Yang et al., 2020). Model's hyperparameters can be fine-tuned to find values that give the best model accuracy.

With the aim to determine values of model's hyperparameters as accurately as possible, I performed nested spatial cross-validation. This method is an extension of previously described approach, with hyperparameter tuning added to the process. Each fold created in the spatial CV is further divided into next n folds which comprise the tuning level of the process. Then, another n -fold cross-validation is performed on these folds in order to determine performance of randomly sampled hyperparameter values. The best hyperparameter combination is chosen to train the model on outer fold (performance estimation level) (Schratz et al., 2019). Whole process is then repeated on every of k outer folds which leads to the most accurate performance measurement as well as defining the best hyperparameter setting.

I chose three hyper-parameters for tuning: number of trees, maximum depth of the tree and minimal size of each node in decision tree. I used overall accuracy achieved by each classifier to rank their performance and choose parameters that train the model best. On the tuning level of every fold in spatial CV process, I examined 10 random configurations of hyperparameters and assessed their performance by applying 5-fold inner resampling. Parameters' search spaces and tuning result received from nested cross-validation can be found in Table 2.3.

2.4 Variable importance and its spatial distribution

Quantifying importance of model's variables is a part of evaluating its results. It can be used for model simplification and exploration, domain-knowledge-based validation or knowledge generation (Biecek et al., 2021). This study was focused on the latter purpose since its aim was to check if thermal information has a significant impact on land cover classification.

Importance of model variables can be measured on two levels: dataset level and instance level (Biecek et al., 2021). On the dataset level, we can measure change in model accuracy depending on the presence of one chosen variable (Section 2.4.1). This gives basic knowledge about this variable's impact on model predictions. Assessing importance on the instance (observation) level helps to understand an impact of variables for one specific data point (Section 2.4.2). Moreover, the instance level importance can be utilized to interpolate variable importance values from points into continuous raster data (Section 2.4.3).

2.4.1 Dataset level

Measuring variable importance on the dataset level requires evaluating model twice: once with original data and once with permuted values of the considered variable. The main idea behind this action is to measure difference between models' performance. Breiman (2001) assumes that if a variable is important, then model's performance is expected to lower after permuting this variable's values. For this purpose, cross entropy was used as a loss function thus its change was considered as a measure of variable importance (Biecek et al., 2021). In order to measure each variable's importance, twelve separate models were created: one with original data and eleven modified models, each one with different variable's values permuted. Comparison of these eleven models and the original model made possible quantifying impact of every variable on the original model results. This value is treated as an overall variable importance on the dataset level.

There is also a visual method to explore variable importance on dataset level. It is based on interpreting partial-dependence (PD) profiles of variables (Figure 2.6). Such plot shows how does probability of choosing certain class changes as a function of the selected variable (Biecek et al., 2021). Values for PD profile are calculated by averaging Ceteris-paribus profiles created for every observation in the dataset. This approach is an easy and intuitive way to understand variables' impact on model results. If probability values of choosing certain class do not change along with the changes of variable's value, we can assume that this variable does not have big impact on model predictions or that our model did not detect such dependence.

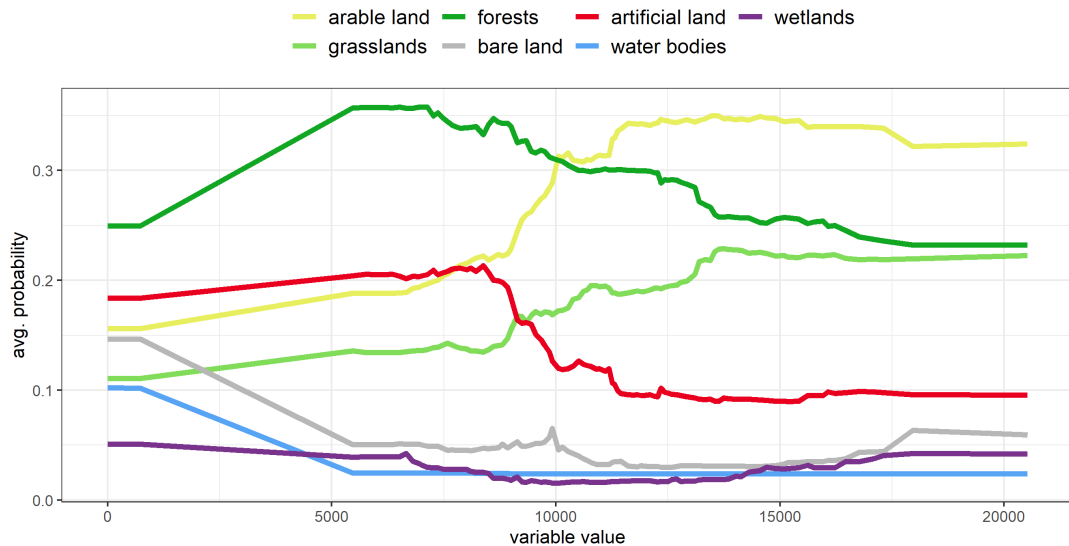


Figure 2.6: Example partial-dependence profile for near-infrared band (B5)

2.4.2 Instance level

Another way to measure variable importance in machine learning models is the instance level evaluation. It helps to find out how much each variable contributed to the model's outcome for a particular observation (Biecek et al., 2021). One way of calculating variable impact on the observation result is creating a break-down plot (Figure 2.7). Its main idea is to estimate contribution of variable by measuring the change in model predictions while fixing the values of consecutive variables to values recorded for the chosen observation (Biecek et al., 2021). After fixing the value of variable for whole

dataset, change in model prediction is calculated. This value indicates the variable impact on a chosen observation.

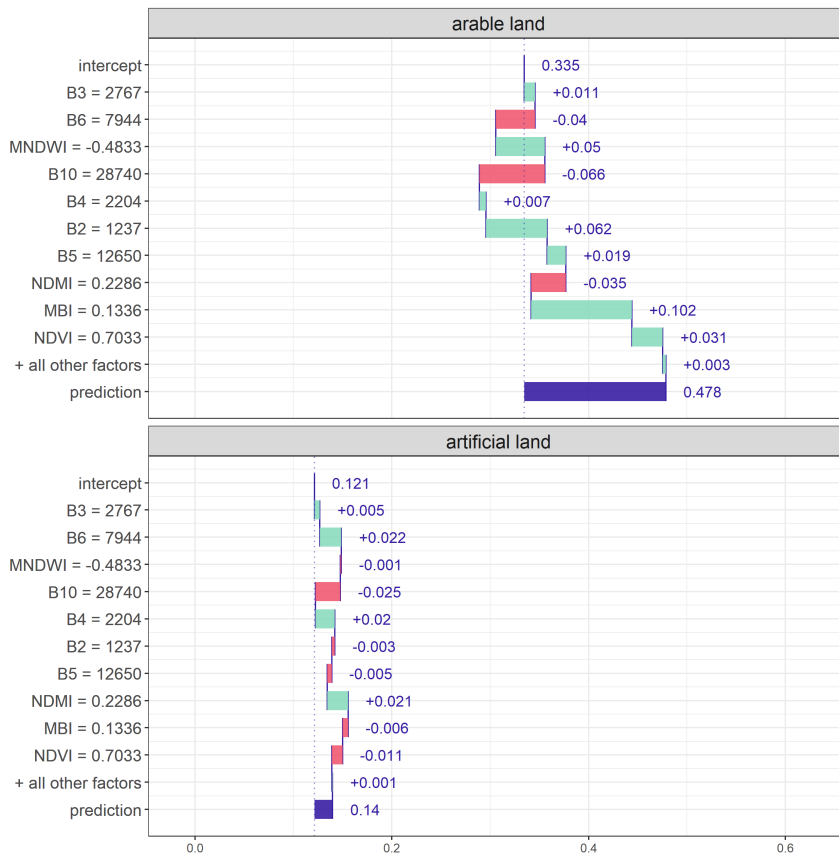


Figure 2.7: Example of a break-down plot that visualises variables' impact on chosen observation

However, above method is highly dependent on variable ordering and interactions between these variables (Biecek et al., 2021). To address this issue, I applied another approach based on averaging values from multiple break-down plots, each one with different ordering of the variables. This method originates from “Shapley values” (Shapley et al., 1953) and was adapted to machine learning by Štrumbelj and Kononenko (2010). Main idea of this approach is to apply several different variable orderings, create a break-down plot for each of them and calculate the mean value of contribution for each variable (Figure 2.8). Thanks to this method, the influence of variable ordering can be mostly removed (Biecek et al., 2021).

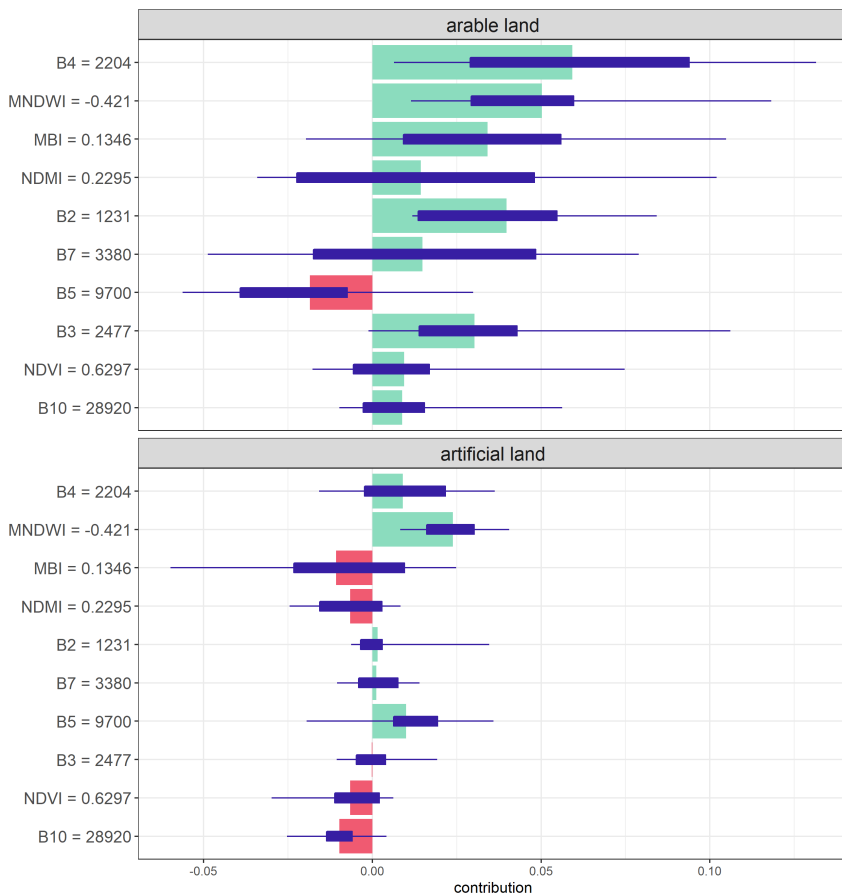


Figure 2.8: Example plot of Shapley Additive Explanations. Green and red bars show average variable contribution to model result. Blue box plots show distribution of variable contributions across different variable orderings.

Eventually, Shapley values provide a possibility to measure contribution of each variable in every observation in the training set. Such result enables us to add spatial context to the variable importance, which is further described in Section 2.4.3.

2.4.3 Spatial distribution

In order to estimate spatial distribution of variable importance values, I applied two different approaches. First of them is based on the raster aggregation - resampling of satellite imagery from 30 m to 1.5 km resolution. Lowering the resolution of the data and averaging band values highly decreases computational time, as well as helps to discover more general trends and patterns rather than local ones. After resampling, Shapley values were calculated for every raster cell and variable importance was measured.

The second approach utilizes LUCAS training points used during a model training together with spatial interpolation techniques. First, Shapley values are calculated for every point and importance of variable is assigned to them. This step is followed by spatial interpolation of variable importance values from points to continuous raster layer with the help of the Inverse Distance Weighting (IDW) interpolation method.

Both approaches have their pros and cons. Raster aggregation method is spatially more consistent, but averaging of spectral values may not entirely represent objects on the ground. On the other hand, point interpolation method is very accurate for places near LUCAS points location, but values for more distant areas may not be as reliable.

2.5 R language environment

Almost every step of analysis described in previous sections was performed with the use of R (R Core Team, 2021) - an open-source programming language designed mainly for statistical computing and visualizing data. I used RStudio (RStudio Team, 2020) as an integrated development environment (IDE). Apart from base R functionalities, a number of packages created by the R community were implemented into workflow. I used *terra* package (Hijmans, 2022) to perform raster data operations and *sf* (Pebesma, 2022) to manipulate and process vector data. To conduct machine learning steps of the analysis, I used an environment of various machine learning packages called *mlr3* (Lang et al., 2022). Random forest algorithm used by *mlr3* framework is part of the *ranger* package (Wright et al., 2021). I also used *dplyr* (Wickham et al., 2022) and *tidyverse* packages (Wickham, 2021) to clean and process tabular data. *DALEX* (Biecek et al., 2022) and *DALEXtra* (Maksymiuk et al., 2022) packages provided various functionalities enabling me to estimate variable importance and visualize these results with the help of the *ggplot2* package (Wickham et al., 2021). Moreover, the *corrplot* package was used to calculate and visualize correlation matrix of Landsat data in order to explore dataset in more detail. Package called *gstat* (Pebesma et al., 2021) helped to interpolate variable importance values from points to a continuous raster layer. In addition, the *future* package (Bengtsson, 2021) was used to enable multi-threading of some computationally intensive tasks.

Chapter 3

Land cover map

The main product of the model is a land cover map of Poznań metropolitan area (Figure 3.1). Moreover, the created model contains probabilities of choosing each class for every pixel of the raster layer. With the help of this information, a probability map showing model's confidence in its choice of land cover class was created (Figure 3.3). Value of each pixel reflects the highest probability assigned to one of seven land cover classes.

After a visual analysis of Figure 3.1, some conclusions about its general accuracy can be made. Overall distributions of main land cover classes such as urban areas (artificial land), forests, arable land and water bodies, seem to be correctly recognized.

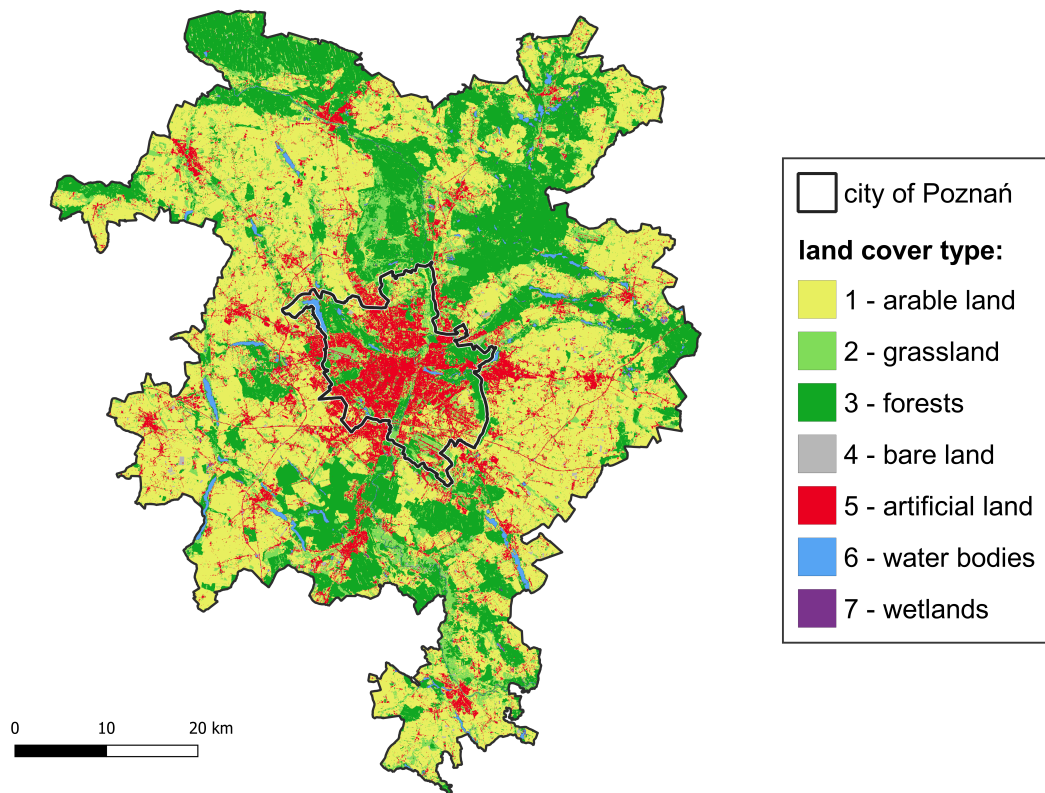


Figure 3.1: Land cover map of Poznań metropolitan area created during this study

In order to investigate model's predictive accuracy on a local scale, six arbitrary chosen sites were examined more closely (Figure 3.2). Locations of sites were selected to present different landscape patterns on the studied map, as well as point out some common mistakes made by the model. Visual analysis of these sites showed that the model correctly recognizes most of land cover patterns present on the ground. At the same time, there were several bigger problems and mistakes in its predictions. For instance, there are many examples of single pixels in the artificial area being classified as arable land (especially in sites 1, 2 and 6). Urban areas on the created map are generally more fragmented than they are in reality. Moreover, some cropland areas were incorrectly classified as grassland (sites 4, 5 and 6). Another problem occurred in the classification of a river surface - its shape on the land cover map was not continuous and water was often misclassified as wetland (sites 1 and 5). On the other hand, the model has managed to correctly recognize wetlands in sites 2 and 4, despite the fact that no training point of wetlands class was located nearby.

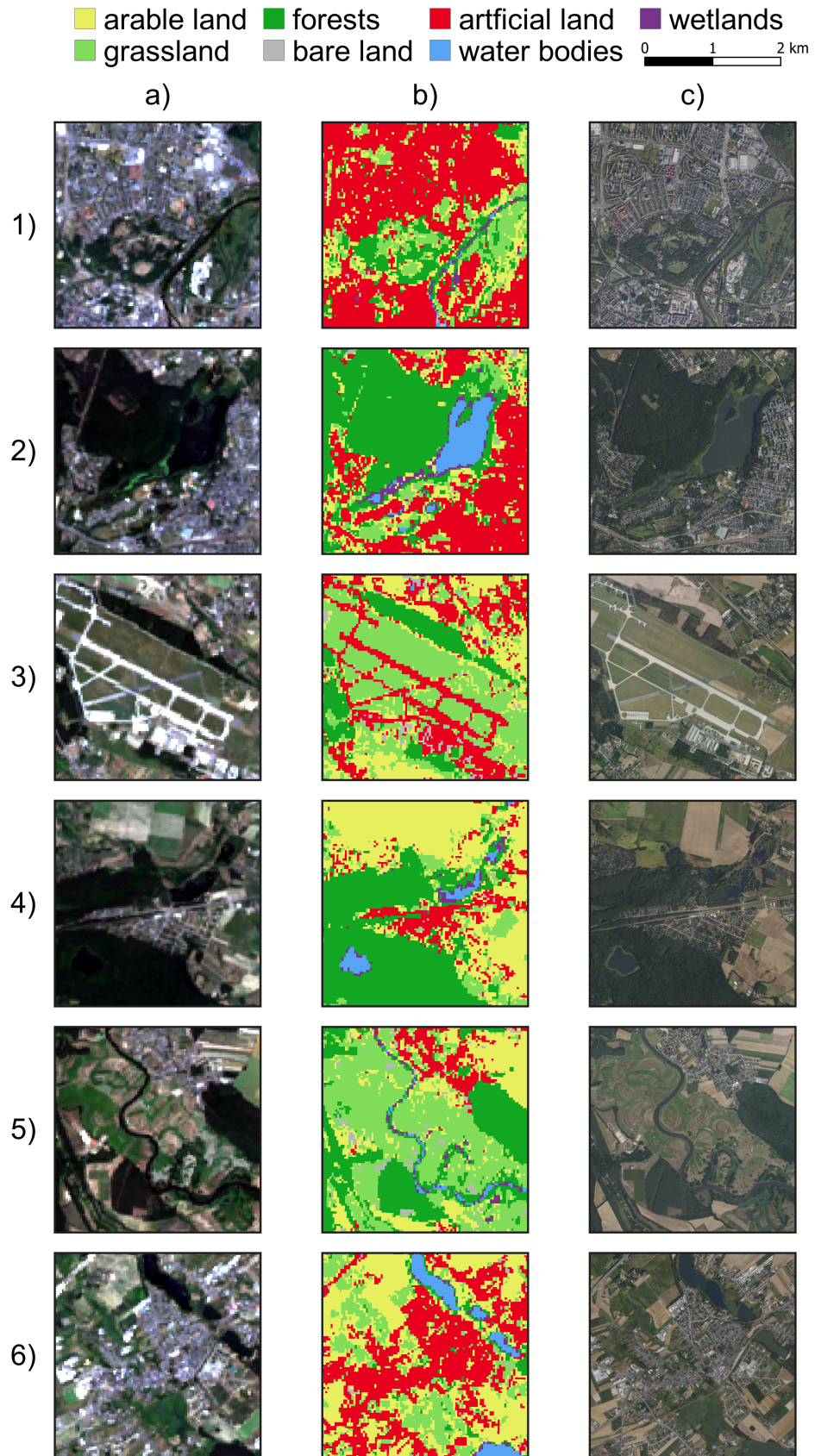


Figure 3.2: Comparison of the created land cover map (b) with GLAD satellite imagery (a) and ortophotomap from Polish Geoportal (c)

Analysis of the model's confidence derived from the probability map (Figure 3.3) showed visible spatial autocorrelation. In order to derive mean values of confidence for every land cover class, zonal statistics were calculated. Highest values of confidence were recorded for forests (0.86) and water bodies (0.92). For urban areas and arable land, model's confidence was lower at mean level of 0.64 and 0.71, respectively. The model was least confident in recognizing bare land (0.44), wetlands (0.46) and grassland (0.57).

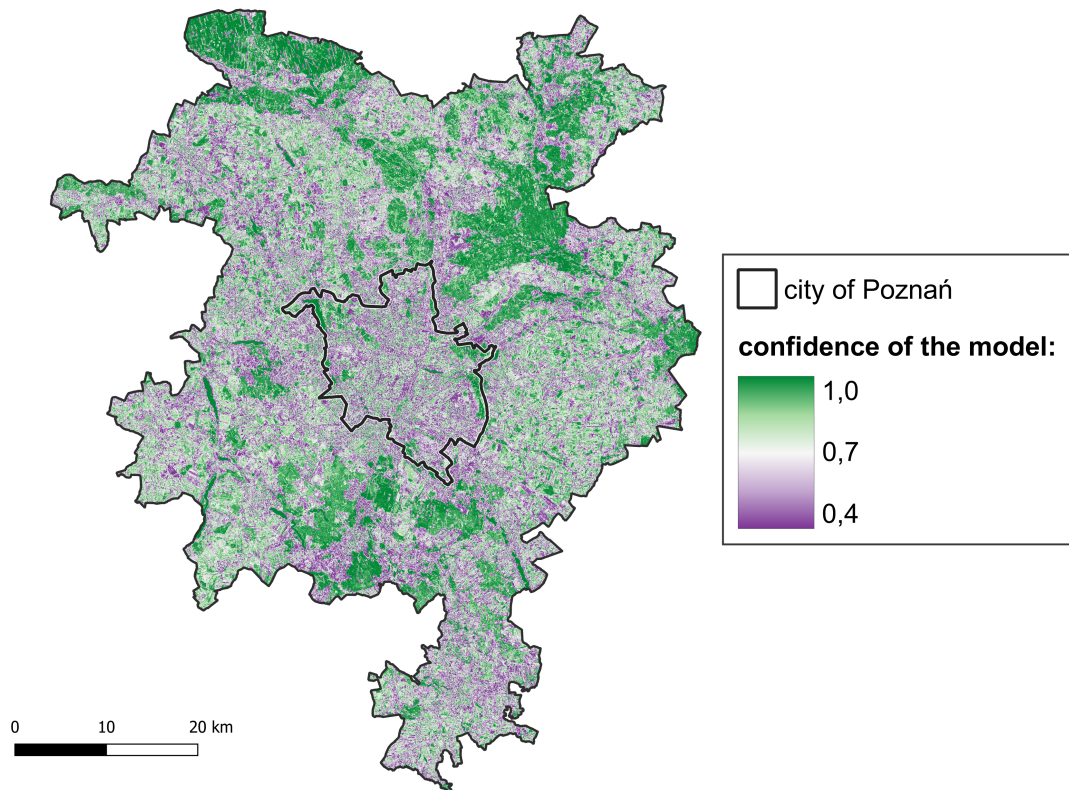


Figure 3.3: Probability of a chosen land cover class being present on the ground. This can be treated as a confidence of the model on its results.

Chapter 4

Assessing model quality

As mentioned in Section 2.3.2, in order to evaluate model performance nested k -fold spatial cross-validation was performed. I chose approach with 5 folds and 10 repetitions. Hyperparameter tuning level of nested resampling used 5 folds to evaluate 10 different hyperparameter combinations. This resulted in total of 2500 models created both for performance estimation and hyperparameter tuning. Results of these models were then evaluated and quality measures were computed. In Table 4.1, overall quality measures, such as, accuracy and Kappa coefficient are presented. Moreover, I calculated weighted precision, recall and F1-score. Weights for these calculations were based on number of observations from each land cover class. Original precision, recall and F1-score values by land cover type are shown in Table 4.2.

In general, model achieved accuracy level of 0.752 with the Kappa coefficient of 0.652. These values are rather average and model indeed needs some improvements. On the other hand, this performance is enough to assess thermal band's importance (Chapter 5), which is the main goal of this study.

An in-depth analysis of performance measures by land cover class shows that precision and recall values for certain type are similar (Table 4.2). This means that model did not have any specific problem either with too many false positive (FP) or false negative (FN) predictions. It was just not that good for some classes. Model performed very poorly in terms of correctly classifying observations of wetlands class but it is quite

Table 4.1: Overall performance measures calculated during cross-validation/resampling process

| Measure | Average value |
|------------------------------|---------------|
| overall accuracy | 0.752 |
| Kappa coefficient | 0.652 |
| precision (user's accuracy) | 0.742 |
| recall (producer's accuracy) | 0.751 |
| weighted F1-score | 0.743 |

Table 4.2: Performance measures by land cover class

| Land cover class | Recall (producer's accuracy) | Precision (user's accuracy) | F1-score |
|------------------|------------------------------|-----------------------------|----------|
| arable land | 0.732 | 0.828 | 0.777 |
| grasslands | 0.612 | 0.613 | 0.612 |
| forests | 0.886 | 0.892 | 0.889 |
| bare land | 0.320 | 0.194 | 0.242 |
| artificial land | 0.656 | 0.493 | 0.563 |
| water bodies | 0.971 | 1.000 | 0.985 |
| wetlands | 0.394 | 0.121 | 0.185 |

common issue across many studies (for example, Malinowski et al. (2020)). Also bare land class had low values of model quality with F1-score of 0.242. The main problem concerning these land cover classes is that there was probably not enough training points for each of them in the study area. On the other hand, two largest classes in terms of number of observations - arable land and forests - were classified much more accurately, with F1-score of 0.777 and 0.889 respectively. Land cover type with the highest values of precision and recall, despite of low number of observations, was the water bodies class. Model performed very good for this class probably because of its distinct spectral characteristics and easily distinguishable borders.

Chapter 5

Evaluating thermal band's impact

As described in Section 2.4, variable importance can be assessed both on dataset and instance (observation) level. The latter was used to estimate spatial distribution of thermal band's importance in order to present the results on the map.

However, before moving to thermal band's importance assessment, I explored Landsat dataset more carefully in order to determine correlated variables and interactions between them (Figure 5.1). Creating correlation plot (Figure 5.1) revealed that some bands are highly correlated - especially these from visible spectrum and SWIR bands. This may suggest that these variables depend on the other variable's values (Biecek et al., 2021), thus absence of one variable might not lower model's performance because other variable can fill this information gap. On the other hand, feature selection performed with the help of *mlr3* framework (Lang et al., 2022) has shown that including all variables still proves to achieve the best model performance. Moreover, implemented methods of assessing variable importance (described in Section 2.4) are designed to minimize impact of interactions between variables.

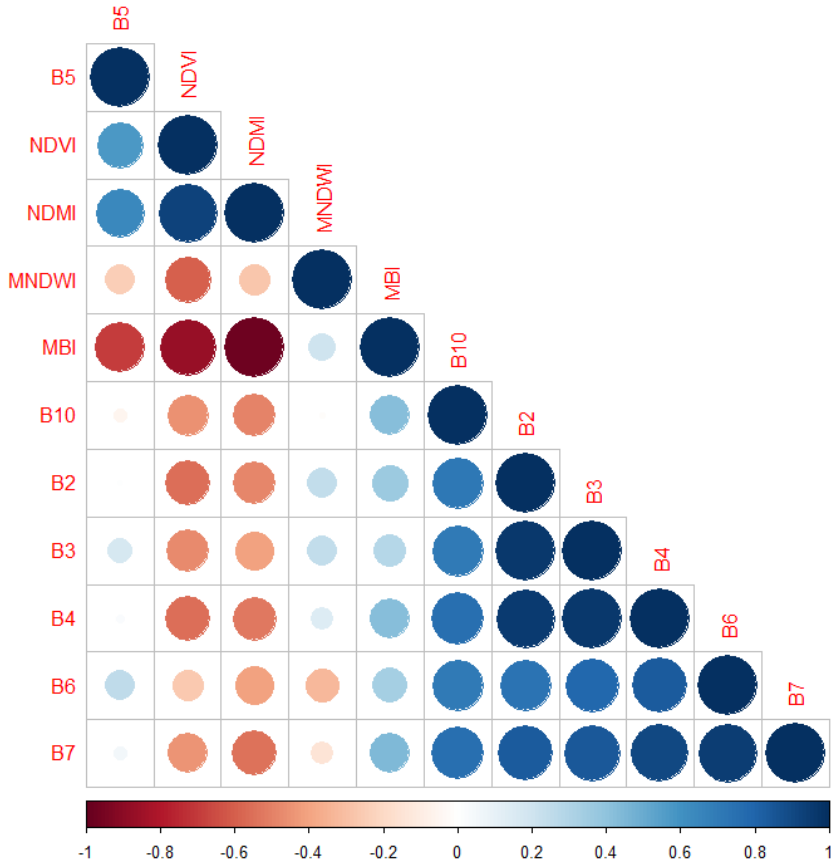


Figure 5.1: Correlation matrix of Landsat bands

5.1 Measuring importance of thermal band

As a very basic way to check thermal band's importance on model results, I implemented benchmarking methods with the help of functions provided by *mlr3* framework (Lang et al., 2022). Two datasets (*tasks*) were created: one with thermal band included and one without this variable. Other hyperparameters of models were the same. Then, 5-fold spatial cross-validation with 10 repetitions were performed on models created from both datasets in order to estimate their predictive abilities. Differences between them were very narrow, but visible - model with thermal band included achieved higher average accuracy of approximately 0.4 perc. points and higher average Kappa of approx. 0.006. Moreover, distribution of accuracy values in the boxplot changed visibly, with higher median accuracy for model with thermal band included (Figure 5.2). In the end,

however, these differences are rather small and we can not state that thermal band had strong impact on model predictions.

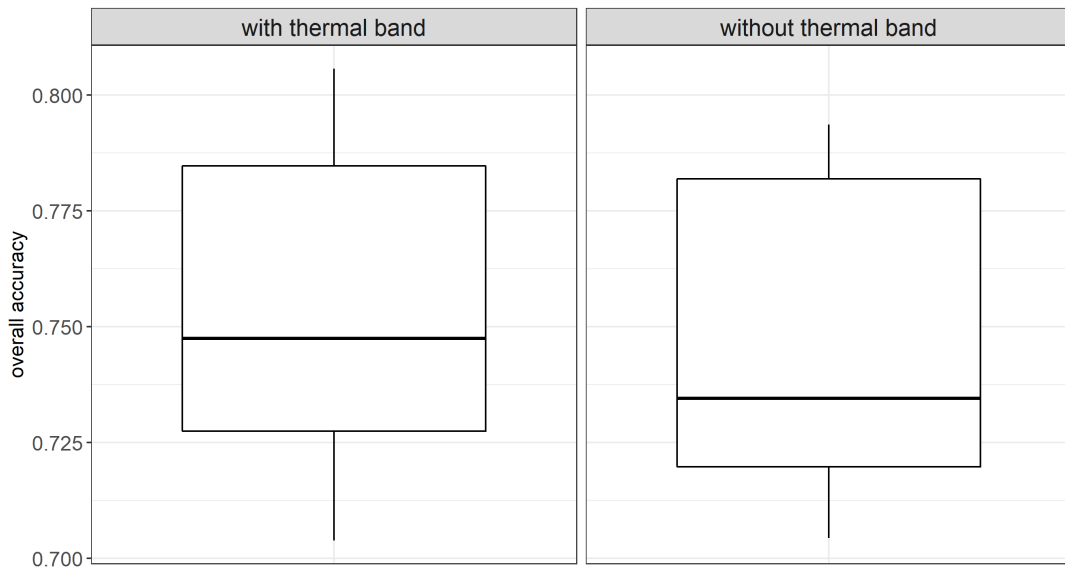


Figure 5.2: Accuracy distributions for 50 models with and without thermal band included

In the next step of thermal information importance evaluation, overall measures were derived. Again, it turned out that thermal band variable had little impact on the model results. With cross-entropy loss value of 28, it was the least important variable in the dataset. Importance values of all variables are shown in Figure 5.3.

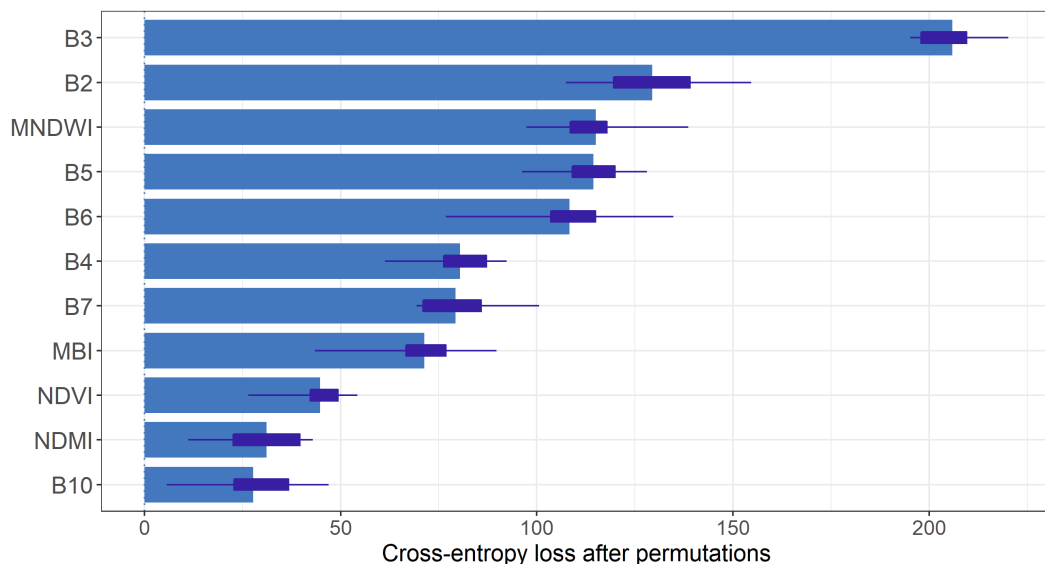


Figure 5.3: Overall variable importance expressed as cross-entropy loss

Table 5.1: Mean value and importance of thermal band, by land cover class of LUCAS points

| Land cover class | Mean temp. [°C] | Average importance | Median importance |
|------------------|-----------------|--------------------|-------------------|
| arable land | 20.5 | 0.022 | 0.019 |
| grasslands | 20.5 | 0.020 | 0.016 |
| forests | 16.0 | 0.022 | 0.019 |
| bare land | 21.1 | 0.019 | 0.019 |
| artificial land | 21.9 | 0.046 | 0.046 |
| water bodies | 13.8 | 0.008 | 0.008 |
| wetlands | 15.0 | 0.049 | 0.016 |

After evaluating variable importance on dataset level, instance level calculations were performed. Shapley values for each of 166 LUCAS points in Poznań metropolitan area were computed and thermal band's importance was derived. This made possible to calculate average thermal band's importance for each of seven land cover classes. In addition, mean value of temperature for each class was computed in order to give better insight into differences between them. Results of these computations are shown in Table 5.1. However, it must be emphasized that 166 points was rather small number, especially for less numerous classes such as wetlands.

Table 5.1 presents differences of thermal band's importance across land cover types. It was significantly higher for artificial land and wetlands. Average value for wetlands is not very reliable though, because there were only 3 such points in studied area - one of them having much higher value of importance than the other two. Due to this issue, median value of importance was calculated too. In this case, value for wetlands was much lower, but importance value for artificial areas was nearly the same. Distributions of importance values can be examined in larger detail in Figure 5.4.

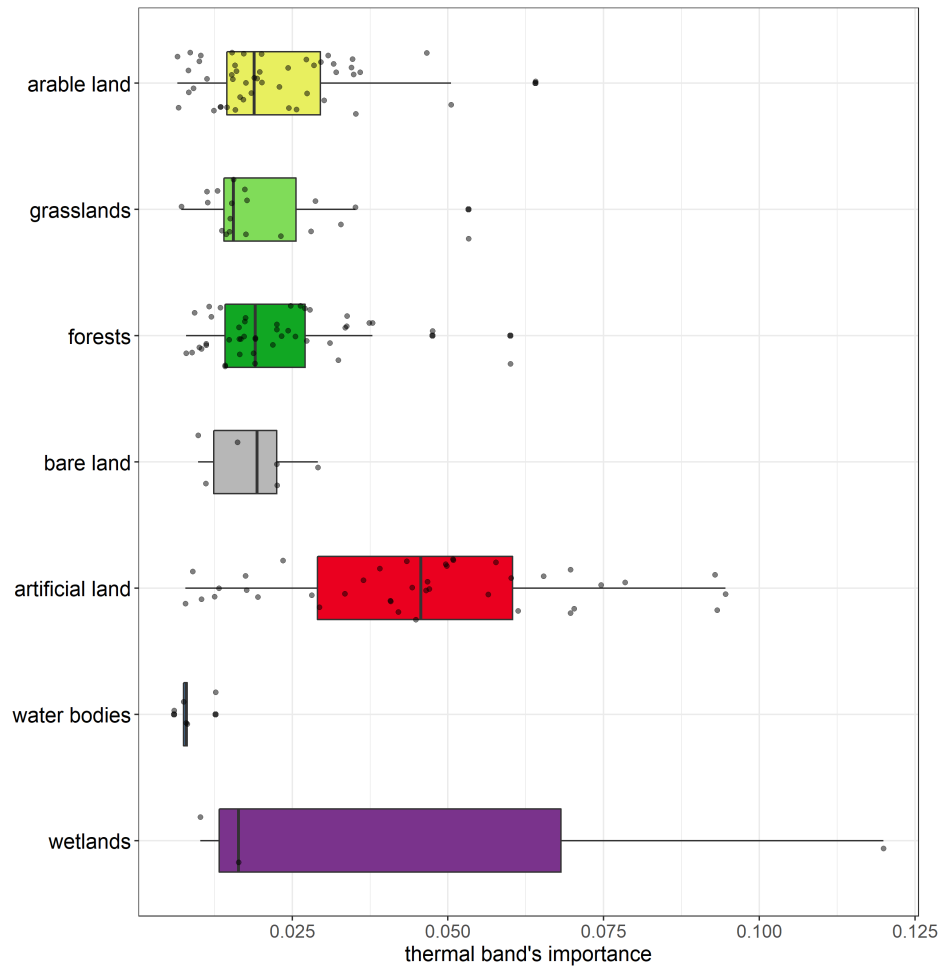


Figure 5.4: Distributions of thermal band's importance by land cover class. Small dots show exact values of each LUCAS point.

In addition, mean importance values for every land cover class are shown in Figure 5.5. With the help of this chart, some comparisons between land cover classes and variables can be made. Thermal band's importance for prediction of artificial land turns out not to be the highest among other variables. Some bands have higher influence on predicting this land cover type. On the other hand, thermal band is one of five bands, whose impact for predicting artificial land was higher than the average.

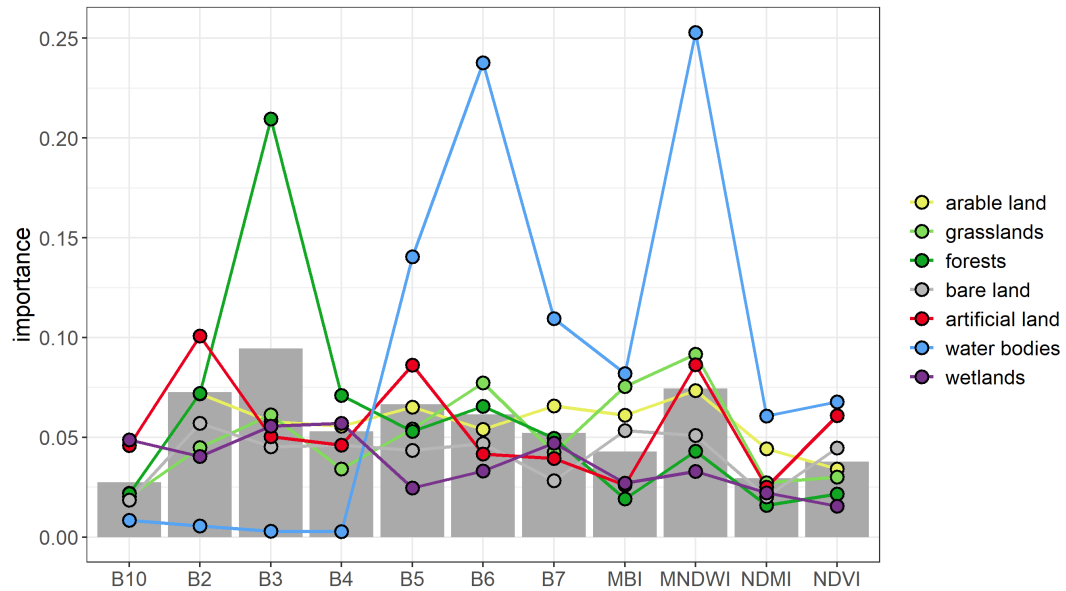


Figure 5.5: Comparison of variable importance values by land cover class and variable. Grey bars show average value of importance of a variable.

In the last step of evaluating thermal band's impact for the model, I created partial-dependence (PD) profiles for this variable (Figure 5.6) and compared it with PD profile for near-infrared band (B5) presented in Figure 5.7. Thanks to PD plots, I checked how probability for choosing certain class changed with increasing values of analysed variables while keeping other features at their average values. Probabilities do not drastically change with temperature (thermal band's value) increase, there are only small fluctuations for several classes. This allows us to conclude that thermal band might not have significant impact on model results. In contrast, B5 variable profile has clearly visible fluctuations for nearly every class (Figure 5.7). Probabilities change significantly along with changes of near-infrared values, thus suggesting that this variable has greater impact on the model predictions than thermal band.

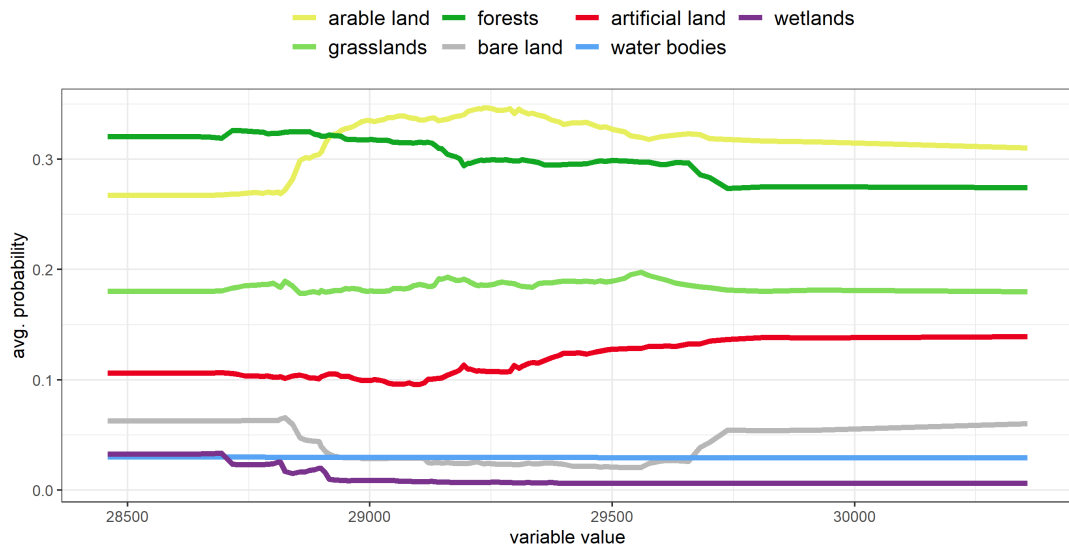


Figure 5.6: Partial-dependence profile for thermal band (B10)

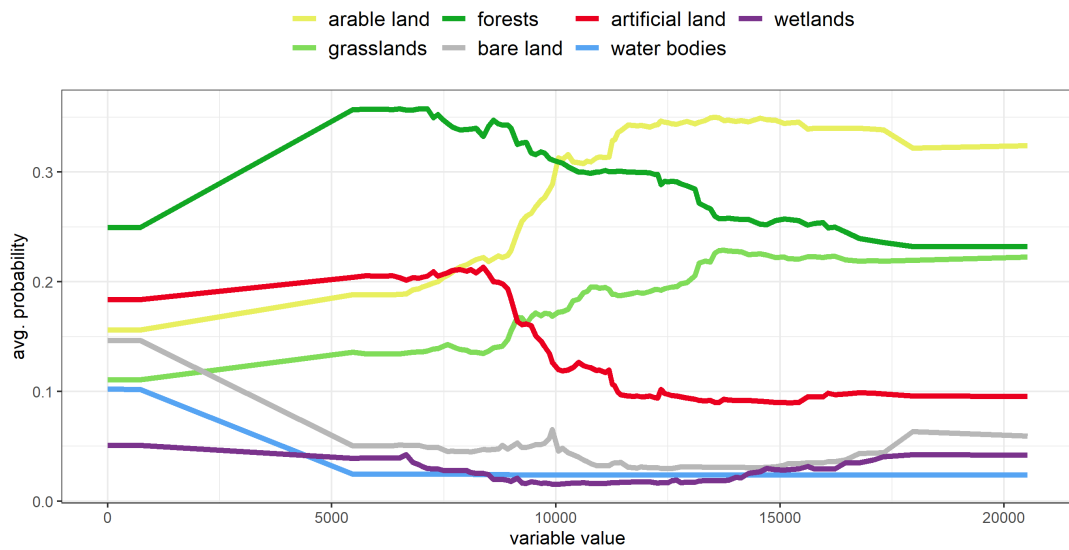


Figure 5.7: Partial-dependence profile for near-infrared band (B5)

5.2 Spatial distribution of thermal band's importance

Variable importance values computed for LUCAS points in Section 5.1 were used to interpolate them into continuous raster layer using IDW interpolation method. This step created an opportunity to examine approximate spatial distribution of thermal band's importance across Poznań metropolitan area (Figure 5.8).

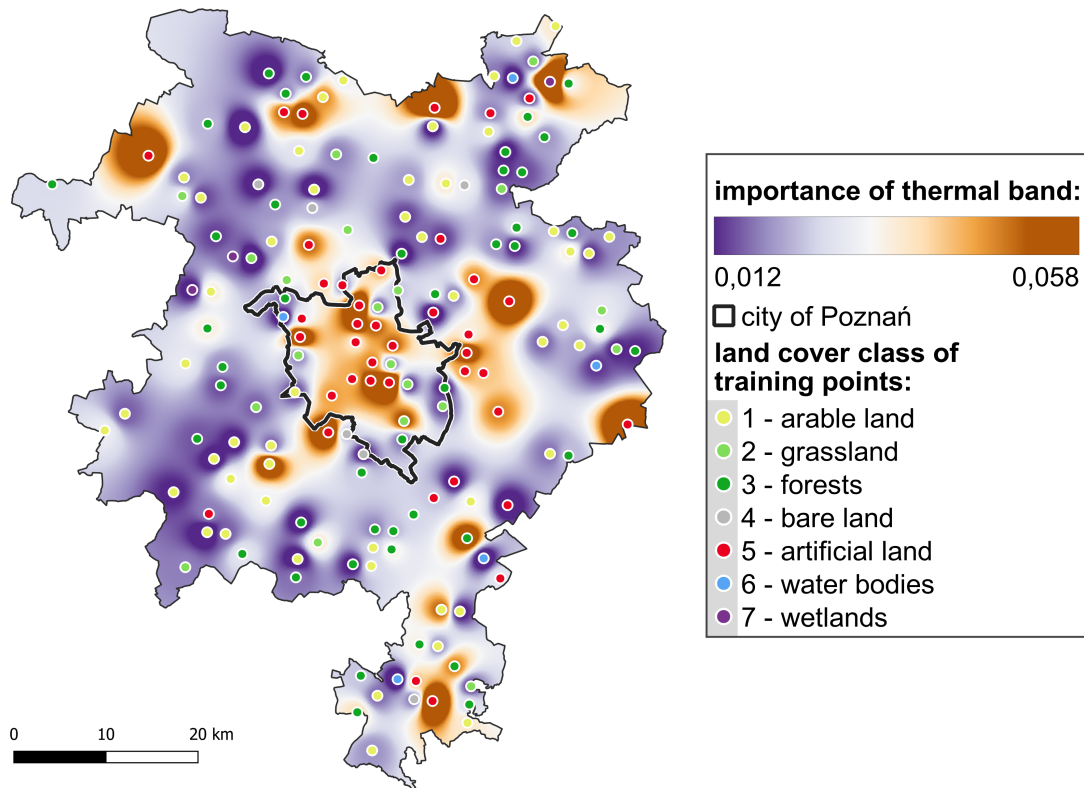


Figure 5.8: Thermal band importance interpolated from values on LUCAS points locations

Moreover, alternative approach involving raster aggregation was also implemented. In this method, original satellite data was aggregated (resampled) to 1,5 km resolution in order to make analysis more general and to shorten the computation time. After aggregation, thermal band's importance was calculated for every raster cell. Result of these calculations, as well as aggregated raster in RGB composition, are shown in Figure 5.9. In general, there is similar distribution of thermal band's importance like in Figure 5.8, however this approach does not require interpolation of values from points which may be misleading, especially in places far away from LUCAS points. On the other hand, spectral values were averaged for every 1,5 km cell so these mean values may not represent accurately features on the ground.

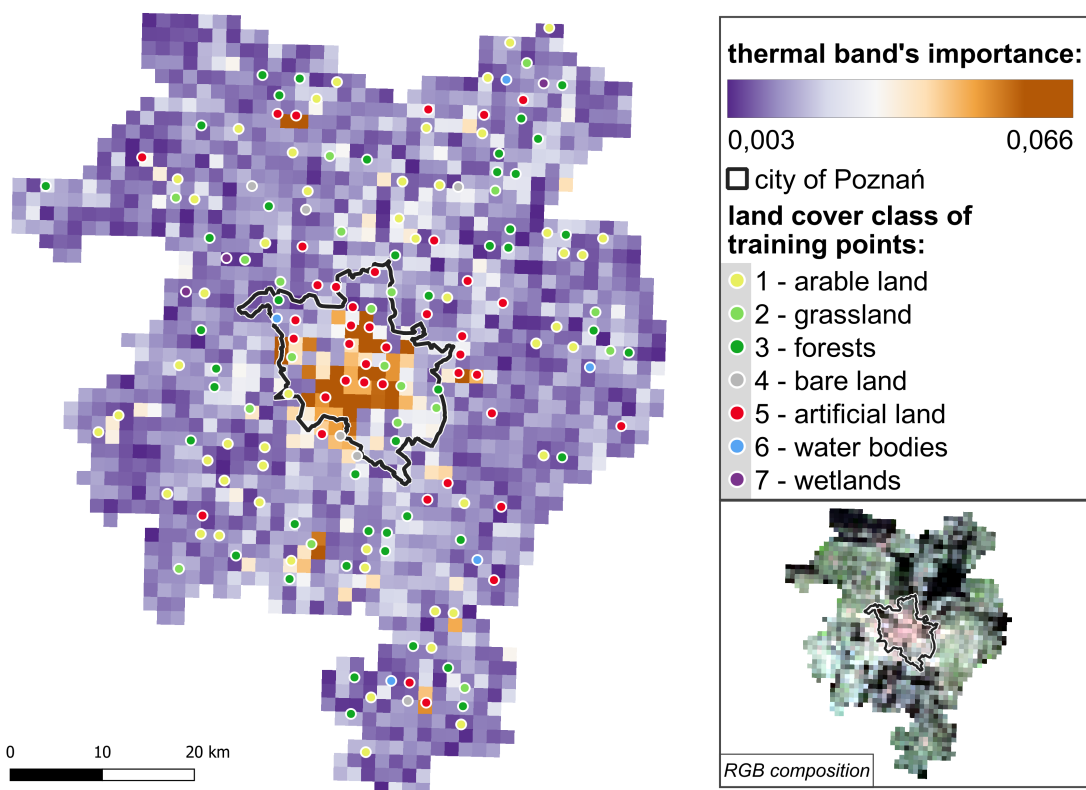


Figure 5.9: Thermal band importance calculated for raster cells aggregated to 1,5 km resolution. Small map in right-bottom corner shows averaged spectral values in RGB composition.

Correlation of thermal band's importance with artificial land class is visible on both maps. In each case, high importance values are concentrated mainly in urban areas, especially in Poznań as it is the biggest city in the study area. Also in smaller towns there is a higher thermal band's impact on model results, but because of their size, it is often harder to detect.

Chapter 6

Conclusions

This study showed that thermal band's impact on machine learning model results is not very strong overall and quantifying its importance needs more in-depth approach. The land cover map was created from imagery of only one 16-day interval and its accuracy was rather average, especially when compared with state-of-the-art works in this field (Malinowski et al., 2020; Witjes et al., 2021). On the other hand, obtained results were accurate enough to apply methods of measuring variable importance and to make some conclusions from findings of this analysis.

In order to add spatial context to the importance values, two methods of creating variable importance maps were developed in my work. The first method applied points interpolation, while the second one used raster aggregation and averaged spectral values. After analysis of the created maps, it became clear that thermal band was more influential in classifying urban areas than for rest of the classes, although its importance was mostly correlated with land cover type. Clear spatial-autocorrelation of thermal band's importance was not detected, probably because of too sparsely distributed training points. Above method should be further examined and tested, since studying spatial distribution of variable importance could improve our understanding of different variables' impact on machine learning model results or may provide new knowledge in this topic.

The most substantial difference between this work and previous studies on the topic is the scope of variable importance evaluation. Both Rodríguez-Galiano et al. (2012) and Zhao (2019) used only variable importance estimation built into the Random Forest algorithm. Sun and Shulz (2015) analysed an increase of overall accuracy (OA) of the model only. In contrast, variable importance was evaluated in this study using several methods such as permutation-based computation, break-down plots, Shapley values and partial-dependence profiles (Section 2.4). All these approaches gave similar outcomes - thermal band had low impact on the general results of the created model. Inclusion of thermal band increased overall performance measures by a very narrow margin (less than 1%), which is not as optimistic outcome as in previously mentioned studies (Rodríguez-Galiano et al., 2012; Sun et al., 2015; Zhao et al., 2019). All these works estimated impact of thermal band on overall accuracy at 2-10%. However, more in-depth analysis revealed that land surface temperature had greater impact on predicting artificial land than any other land cover class. Also Rodríguez-Galiano et al. (2012) and Zhao (2019) discovered that thermal band improves classification of artificial areas. On the other hand, my results does not confirm other finding of Zhao (2019), stating that thermal band helps in distinguishing arable land from wetlands - this divergence is probably caused by entirely different environments of study areas, Egypt and Poland.

Findings of my study suggest that thermal band could help in mapping the development of cities and urban areas. Its inclusion may help distinguish an artificial land from other similar land cover types. More accurate land cover maps will help in better growth management of metropolitan areas and in quantifying impact of urbanization on natural environment more precisely. Nonetheless, further research should be carried out on bigger area and for larger number of satellite images. It is crucial to extend this study to include spatio-temporal aspect of imagery, in order to investigate thermal band's impact on model predictions throughout different vegetation seasons. Moreover, areas from different climate zones should be examined with an emphasis on the thermal band importance issue. Newly launched Landsat 9 satellite can also provide improvement for thermal band's use for land cover mapping, because its thermal sensor is expected to perform better in Earth observation than its predecessor from Landsat 8.

Bibliography

- Bengtsson, H (2021). *future: Unified Parallel and Distributed Processing in R for Everyone*. R package version 1.23.0. <https://CRAN.R-project.org/package=future>.
- Biecek, P and T Burzykowski (2021). *Explanatory Model Analysis*. Chapman and Hall/CRC, New York. <https://pbiecek.github.io/ema/>.
- Biecek, P, S Maksymiuk, and H Baniecki (2022). *DALEX: moDel Agnostic Language for Exploration and eXplanation*. R package version 2.4.0. <https://CRAN.R-project.org/package=DALEX>.
- Bojinski, S, M Verstraete, TC Peterson, C Richter, A Simmons, and M Zemp (2014). The Concept of Essential Climate Variables in Support of Climate Research, Applications, and Policy. EN. *Bulletin of the American Meteorological Society* **95**(9). Publisher: American Meteorological Society Section: Bulletin of the American Meteorological Society, 1431–1443. (Visited on 01/24/2023).
- Breiman, L (2001). Random Forests. *Machine Learning* **45**(1), 5–32.
- Brenning, A (2012). Spatial cross-validation and bootstrap for the assessment of prediction rules in remote sensing: The R package sperrorest. en. In: *2012 IEEE International Geoscience and Remote Sensing Symposium*. Munich, Germany: IEEE, pp.5372–5375. <http://ieeexplore.ieee.org/document/6352393/> (visited on 01/03/2023).
- Buck, O, C Haub, S Woditsch, D Lindemann, L Kleinewillingshöfer, G Hazeu, B Kosztra, S Kleeschulte, S Arnold, and M Hödl (2015). *Analysis of the LUCAS nomenclature and proposal for adaptation of the nomenclature in view of its use by the Copernicus land monitoring services*. https://land.copernicus.eu/user-corner/technical-library/LUCAS_Copernicus_Report_v22.pdf.

BIBLIOGRAPHY

- d'Andrimont, R, M Yordanov, L Martinez-Sanchez, B Eiselt, A Palmieri, P Dominici, J Gallego, HI Reuter, C Joebges, G Lemoine, and M van der Velde (2020). Harmonised LUCAS in-situ land cover and use database for field surveys from 2006 to 2018 in the European Union. en. *Scientific Data* 7(1), 352. (Visited on 11/13/2022).
- Dutta, D, A Rahman, SK Paul, and A Kundu (2019). Changing pattern of urban landscape and its effect on land surface temperature in and around Delhi. en. *Environmental Monitoring and Assessment* 191(9), 551. (Visited on 01/24/2023).
- Hashem, N and P Balakrishnan (2015). Change analysis of land use/land cover and modelling urban growth in Greater Doha, Qatar. *Annals of GIS* 21(3). Publisher: Taylor & Francis _eprint: <https://doi.org/10.1080/19475683.2014.992369>, 233–247. (Visited on 01/24/2023).
- Hijmans, RJ (2022). *terra: Spatial Data Analysis*. R package version 1.5-21. <https://rspatial.org/terra/>.
- Jiao, Y and P Du (2016). Performance measures in evaluating machine learning based bioinformatics predictors for classifications. en. *Quantitative Biology* 4(4), 320–330. (Visited on 01/03/2023).
- Jin, S and SA Sader (2005). Comparison of time series tasseled cap wetness and the normalized difference moisture index in detecting forest disturbances. en. *Remote Sensing of Environment* 94(3), 364–372. (Visited on 01/27/2023).
- Kuhn, M and K Johnson (2013). *Applied Predictive Modeling*. en. New York, NY: Springer New York. <http://link.springer.com/10.1007/978-1-4614-6849-3> (visited on 12/20/2022).
- Lang, M, B Bischl, J Richter, P Schratz, and M Binder (2022). *mlr3: Machine Learning in R - Next Generation*. R package version 0.13.3. <https://CRAN.R-project.org/package=mlr3>.
- Lovelace, R, J Nowosad, and J Muenchow (2019). *Geocomputation with R*. CRC Press.
- Mahesh, B (2018). Machine Learning Algorithms - A Review. en. 9(1).
- Maksymiuk, S, P Biecek, and H Baniecki (2022). *DALEXtra: Extension for DALEX Package*. R package version 2.2.0. <https://CRAN.R-project.org/package=DALEXtra>.
- Malinowski, R, S Lewiński, M Rybicki, E Gromny, M Jenerowicz, M Krupiński, A Nowakowski, C Wojtkowski, M Krupiński, E Krätzschmar, and P Schauer (2020).

BIBLIOGRAPHY

- Automated Production of a Land Cover/Use Map of Europe Based on Sentinel-2 Imagery. en. *Remote Sensing* **12**(21), 3523. (Visited on 04/07/2022).
- Maxwell, AE, TA Warner, and F Fang (2018). Implementation of machine-learning classification in remote sensing: an applied review. *International Journal of Remote Sensing* **39**(9). Publisher: Taylor & Francis _eprint: <https://doi.org/10.1080/01431161.2018.1433343>, 2784–2817. (Visited on 01/24/2023).
- Nguyen, CT, A Chidthaisong, P Kieu Diem, and LZ Huo (2021). A Modified Bare Soil Index to Identify Bare Land Features during Agricultural Fallow-Period in Southeast Asia Using Landsat 8. en. *Land* **10**(3). Number: 3 Publisher: Multidisciplinary Digital Publishing Institute, 231. (Visited on 01/27/2023).
- Pebesma, E (2022). *sf: Simple Features for R*. R package version 1.0-7. <https://CRAN.R-project.org/package=sf>.
- Pebesma, E and B Graeler (2021). *gstat: Spatial and Spatio-Temporal Geostatistical Modelling, Prediction and Simulation*. R package version 2.0-8. <https://github.com/r-spatial/gstat/>.
- Pflugmacher, D, A Rabe, M Peters, and P Hostert (2019). Mapping pan-European land cover using Landsat spectral-temporal metrics and the European LUCAS survey. en. *Remote Sensing of Environment* **221**, 583–595. (Visited on 04/14/2022).
- Potapov, P, MC Hansen, I Kommareddy, A Kommareddy, S Turubanova, A Pickens, B Adusei, A Tyukavina, and Q Ying (2020). Landsat Analysis Ready Data for Global Land Cover and Land Cover Change Mapping. en. *Remote Sensing* **12**(3), 426. (Visited on 04/07/2022).
- QGIS Development Team (2009). *QGIS Geographic Information System*. <https://www.qgis.org>.
- Qi, Y (2012). Random Forest for Bioinformatics. en.
- R Core Team (2021). *R: A Language and Environment for Statistical Computing*. R Foundation for Statistical Computing. Vienna, Austria. <https://www.R-project.org/>.
- Rawat, JS and M Kumar (2015). Monitoring land use/cover change using remote sensing and GIS techniques: A case study of Hawalbagh block, district Almora, Uttarakhand, India. en. *The Egyptian Journal of Remote Sensing and Space Science* **18**(1), 77–84. (Visited on 01/23/2023).

BIBLIOGRAPHY

- Reis, S (2008). Analyzing Land Use/Land Cover Changes Using Remote Sensing and GIS in Rize, North-East Turkey. en. *Sensors* **8**(10). Number: 10 Publisher: Molecular Diversity Preservation International, 6188–6202. (Visited on 01/24/2023).
- Rodríguez-Galiano, V, B Ghimire, E Pardo-Igúzquiza, M Chica-Olmo, and R Congalton (2012). Incorporating the Downscaled Landsat TM Thermal Band in Land-cover Classification using Random Forest. en. *Photogrammetric Engineering & Remote Sensing* **78**(2), 129–137. (Visited on 01/24/2023).
- RStudio Team (2020). *RStudio: Integrated Development Environment for R*. Boston, MA. <http://www.rstudio.com/>.
- Running, SW (2008). Ecosystem Disturbance, Carbon, and Climate. en. *Science* **321**(5889), 652–653. (Visited on 01/23/2023).
- Sarker, IH (2021). Machine Learning: Algorithms, Real-World Applications and Research Directions. en. *SN Computer Science* **2**(3), 160. (Visited on 12/15/2022).
- Schonlau, M and RY Zou (2020). The random forest algorithm for statistical learning. en. *The Stata Journal: Promoting communications on statistics and Stata* **20**(1), 3–29. (Visited on 12/20/2022).
- Schratz, P, J Muenchow, E Iturritxa, J Richter, and A Brenning (2019). Hyperparameter tuning and performance assessment of statistical and machine-learning algorithms using spatial data. en. *Ecological Modelling* **406**, 109–120. (Visited on 01/03/2023).
- Sekulić, A, M Kilibarda, GB Heuvelink, M Nikolić, and B Bajat (2020). Random Forest Spatial Interpolation. en. *Remote Sensing* **12**(10), 1687. (Visited on 12/20/2022).
- Shapley, LS, KJ Arrow, EW Barankin, D Blackwell, R Bott, N Dalkey, M Dresher, D Gale, DB Gillies, I Glicksberg, O Gross, S Karlin, HW Kuhn, JP Mayberry, JW Milnor, TS Motzkin, J Von Neumann, H Raiffa, LS Shapley, M Shiffman, FM Stewart, GL Thompson, and RM Thrall (1953). “A Value For N-Person Games”. In: *Contributions to the Theory of Games (AM-28), Volume II*. Ed. by HW Kuhn and AW Tucker. Princeton University Press, pp.307–318. <http://www.jstor.org/stable/j.ctt1b9x1zv.24> (visited on 01/09/2023).
- Sohil, F, MU Sohali, and J Shabbir (2022). An introduction to statistical learning with applications in R: by Gareth James, Daniela Witten, Trevor Hastie, and Robert Tibshirani,

- New York, Springer Science and Business Media, 2013, \$41.98, eISBN: 978-1-4614-7137-7. en. *Statistical Theory and Related Fields* 6(1), 87–87. (Visited on 01/03/2023).
- Strumbelj, E and I Kononenko (2010). An Efficient Explanation of Individual Classifications using Game Theory. en.
- Sun, L and K Schulz (2015). The Improvement of Land Cover Classification by Thermal Remote Sensing. en. *Remote Sensing* 7(7), 8368–8390. (Visited on 04/07/2022).
- Talukdar, S, P Singha, S Mahato, Shahfahad, S Pal, YA Liou, and A Rahman (2020). Land-Use Land-Cover Classification by Machine Learning Classifiers for Satellite Observations—A Review. en. *Remote Sensing* 12(7), 1135. (Visited on 01/24/2023).
- Tobler, WR (1970). A Computer Movie Simulating Urban Growth in the Detroit Region. en. *Economic Geography* 46, 234. (Visited on 01/04/2023).
- Tucker, CJ (1979). Red and photographic infrared linear combinations for monitoring vegetation. en. *Remote Sensing of Environment* 8(2), 127–150. (Visited on 01/27/2023).
- Varga, OG, Z Kovács, L Bekő, P Burai, Z Csatáriné Szabó, I Holb, S Ninsawat, and S Szabó (2021). Validation of Visually Interpreted Corine Land Cover Classes with Spectral Values of Satellite Images and Machine Learning. en. *Remote Sensing* 13(5), 857. (Visited on 04/07/2022).
- Wickham, H (2021). *tidyverse: Tidy Messy Data*. R package version 1.1.4. <https://CRAN.R-project.org/package=tidyr>.
- Wickham, H, W Chang, L Henry, TL Pedersen, K Takahashi, C Wilke, K Woo, H Yutani, and D Dunnington (2021). *ggplot2: Create Elegant Data Visualisations Using the Grammar of Graphics*. R package version 3.3.5. <https://CRAN.R-project.org/package=ggplot2>.
- Wickham, H, R François, L Henry, and K Müller (2022). *dplyr: A Grammar of Data Manipulation*. R package version 1.0.10. <https://CRAN.R-project.org/package=dplyr>.
- Witjes, M, L Parente, CJv Diemen, T Hengl, M Landa, L Brodsky, L Halounova, J Krizan, L Antonic, CM Ilie, V Craciunescu, M Kilibarda, O Antonijevic, and L Glusica (2021). *A spatiotemporal ensemble machine learning framework for generating land use / land cover time-series maps for Europe (2000 – 2019) based on LUCAS, CORINE and GLAD Landsat*. en. preprint. In Review. <https://www.researchsquare.com/article/rs-561383/v1> (visited on 04/07/2022).

BIBLIOGRAPHY

- Wright, MN, S Wager, and P Probst (2021). *ranger: A Fast Implementation of Random Forests.* R package version 0.13.1. <https://github.com/imbs-hl/ranger>.
- Xu, H (2006). Modification of normalised difference water index (NDWI) to enhance open water features in remotely sensed imagery. en. *International Journal of Remote Sensing* **27**(14), 3025–3033. (Visited on 01/27/2023).
- Yang, L and A Shami (2020). On Hyperparameter Optimization of Machine Learning Algorithms: Theory and Practice. en. *Neurocomputing* **415**. arXiv:2007.15745 [cs, stat], 295–316. (Visited on 01/02/2023).
- Zhao, J, L Yu, Y Xu, H Ren, X Huang, and P Gong (2019). Exploring the addition of Landsat 8 thermal band in land-cover mapping. en. *International Journal of Remote Sensing* **40**(12), 4544–4559. (Visited on 04/07/2022).